CHAPTER TEN

Supercapacitive Behaviour of Single-Walled/Multi-Walled Carbon Nanotubes-Metal (Ni, Fe, Co) Oxide Nanocomposites in Acidic and Neutral pH Conditions*

* The publication below resulted from part of the research work presented in this chapter and it is not referenced further in this thesis:

11. **Abolanle S. Adekunle**, Kenneth I. Ozoemena, *Electroanalysis* (Submitted).
12. **Abolanle S. Adekunle**, Kenneth I. Ozoemena, *J. Power Sources* (Submitted).

10.1 Comparative EDX, XPS and FESEM

Figure 10.1 is the EDX profile of the electrodes. The presence of Ni, Co and Fe peaks in (a), (b) and (c) showed that the electrodes were successfully modified with the respective metal nanoparticles while the occurrence of oxygen peaks with very pronounced intensity implies that the electrodes were successfully transformed to their oxide derivatives. The presence of Ni peak on the EDX of Fe is attributed to Ni impurities from the Fe salts and / or SWCNTs since the EDX of the SWCNTs (not shown) indicated presence of Ni impurities. The occurrence of P and Na peaks in the EDX profiles may be attributed to the sodium phosphate buffer solution used for the electrode preparation.

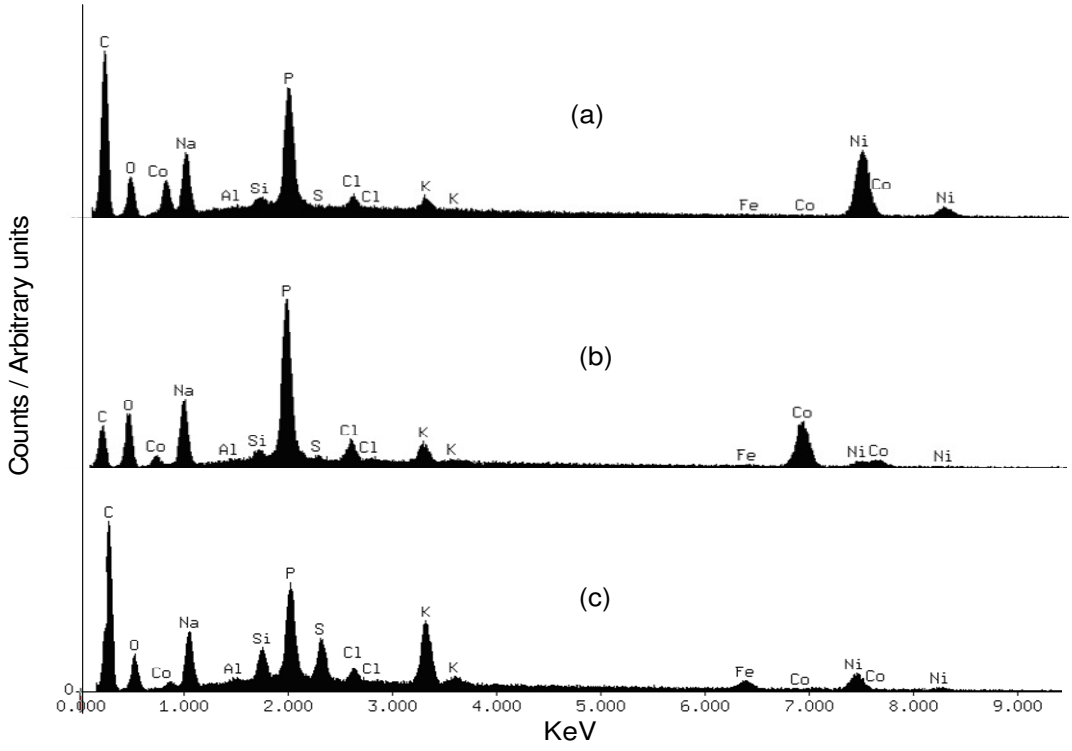

Figure 10.1: EDX spectra of (a) SWCNT-NiO, (b) SWCNT-Co_3O_4 and (c) SWCNT-Fe_2O_3

The XPS data (Figure 10.2) confirmed qualitatively the nature of the species or the oxidation state of the metal nanoparticles in their oxide forms. For example, Ni $2p_{3/2}$ peak at 858.5 eV (Figure 10.2a) is closer to 854.0 eV considered to be NiO [1], which is supported again by the Ni $2p_{1/2}$ peak at 876.0 eV, very close to 873.3 eV observed by Sunohara et al [2]. The Co oxide specimen had $2p_{3/2}$ and $2p_{1/2}$ peaks of Co at 783.0 and 795.7 eV (Figure 10.2b) which is in close agreement with reported values, corresponding to Co_3O_4 [1,3]. The $2p_{3/2}$ and $2p_{1/2}$ peaks at 712.6 and 726.8 eV for Fe oxide modified electrode (Figure 10.2c) agreed with literature value of 710.7 and 724.3 eV which indicates the presence of Fe_2O_3 species [4]. The O1s peak at 532 eV is very close to 530 eV reported to be the lattice oxygen of Fe_2O_3 and Fe_3O_4 [2]. However, the dominant oxide of Fe on the electrode from this result was taken as Fe_2O_3 since species of Fe_3O_4 are not apparent. The Na and the P peaks in Figure 10.2 are attributed to the Na and P of the PBS used during electrode modification while the C peak can be attributed to the carbon of the SWCNTs and the base BPPGE electrode. Hence, the oxides of Fe and Co from this study are taken to be Fe_2O_3 and Co_3O_4 respectively. The metal oxide nanoparticles are porous and somewhat aggregated (Figure 9.3), due possibly to the strong electrostatic interactions between the metal ions and the COO^- charge of the acid-treated SWCNTs. From the SEM image, the average particle size distributions are 20 -50 nm for NiO, 30 – 90 nm for Co_3O_4, and 120 – 200 nm for Fe_2O_3 nanoparticles. Salimi *et al* [5], employed similar method of electrode decoration with cobalt oxide nanoparticles and observed particles agglomeration with sizes ranging from 100 – 600 nm.

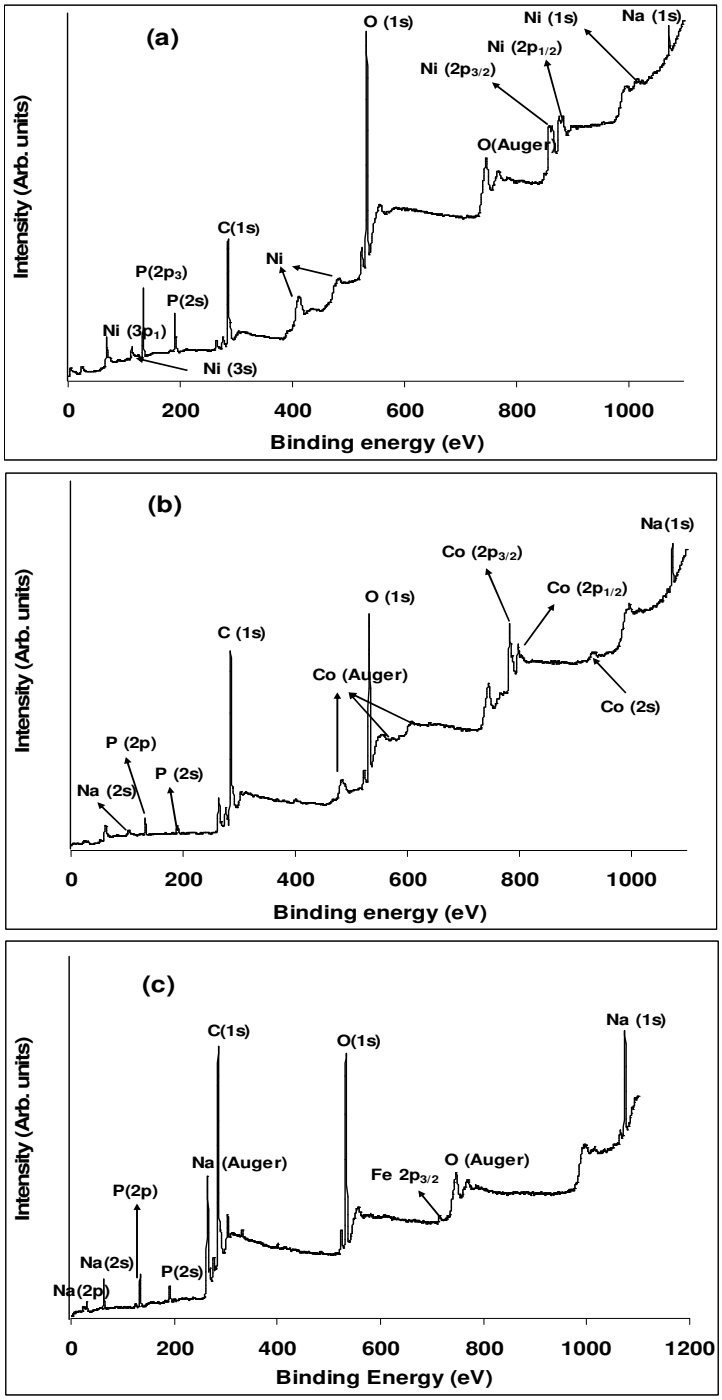

Figure 10.2: XPS spectra of (a) SWCNT-NiO, (b) SWCNT-Co_3O_4 and (c) SWCNT-Fe_2O_3.

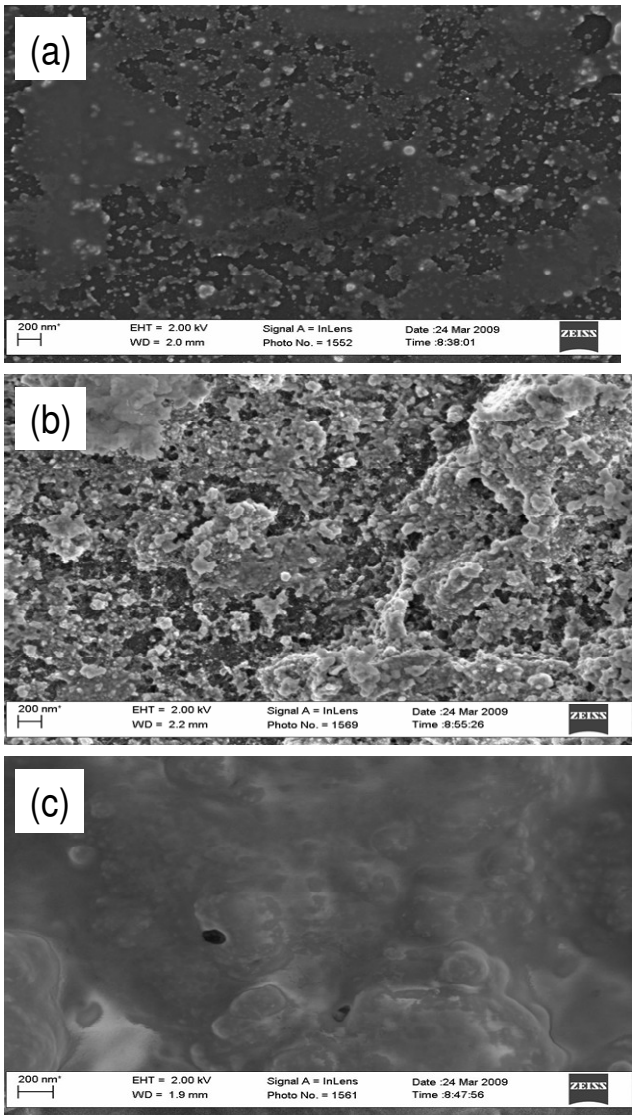

Figure 10.3: FESEM images of (a) SWCNT-NiO (b) SWCNT-Co_3O_4 and (c) SWCNT-Fe_2O_3.

10.2 Comparative cyclic voltammetric experiments

Figure 10.4 presents the comparative CVs of the electrodes in 1 M Na_2SO_4 and 1 M H_2SO_4 solution respectively at a scan rate of 25 mVs^{-1}. The CV indicates several important differences between the composite nanoparticles modified electrodes and the bare BPPGE. First, the SWCNTs exhibit redox couple at $E_{1/2} \approx 0.22$ V and weak oxidation peak at about 0.4 V which may be attributed to the redox processes arising mainly from the oxo-groups at the basal plane sites of the SWCNTs [6]. Second, unlike the voltammograms of the electrodes based on the FeO and CoO nanoparticles, the NiO-based electrodes exhibit huge capacitive current response with irreversible peak around 0.65 V due to the Ni(II)/Ni(III) redox process. The lack of perfect rectangular shape for the curves is attributed to the combination of double layer and pseudo-capacitances contributing to the total capacitance [7]. Third, the capacitive behaviour of the three BPPGE-SWCNT-MO are more pronounced in H_2SO_4 than in Na_2SO_4 electrolyte as can be observed from the charge-discharge study (discussed later).

The ability of the films to store charges may be obtained from the film capacitance (C_{film} / Fcm^{-2}) estimated using the simple expression [8,9]:

$$C_{film}\ (F\ cm^{-2}) = \frac{I_{ch}}{\nu A} \qquad (10.1)$$

where I_{ch} is the average current, ν the scan rate and A the area (cm^2) of the electrode. The equivalent SC values in Fg^{-1} are also estimated and reported (Table 10.1).

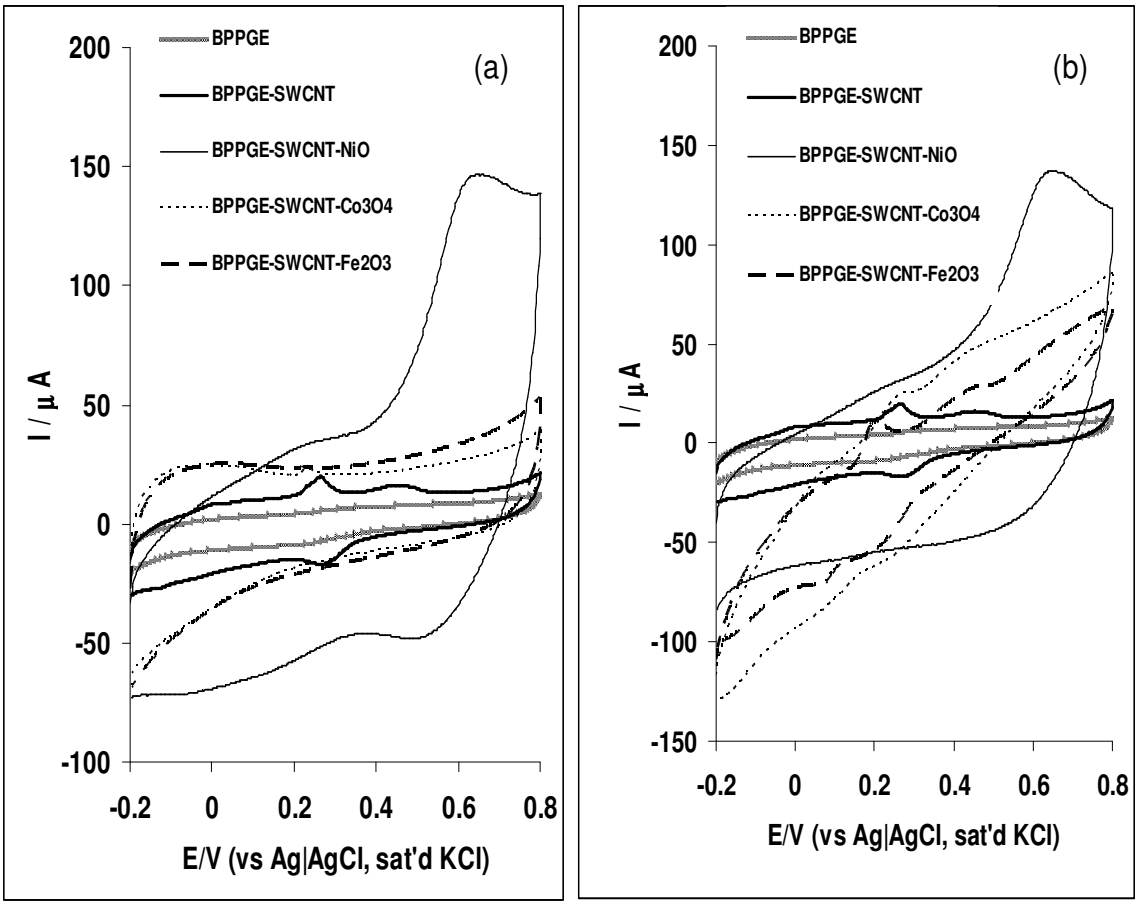

Figure 10.4: Comparative CVs showing the capacitive behaviour of: BPPGE, BPPGE-SWCNT, BPPGE-SWCNT-NiO, BPPGE-SWCNT-Co_3O_4 and BPPGE-SWCNT-Fe_2O_3 in (a) 1 M Na_2SO_4 and (b) 1 M H_2SO_4 aqueous electrolytes. Scan rate = 25 mVs^{-1}.

10.3 Comparative galvanostatic charge / discharge experiments

The ability of the films to store and deliver charges was interrogated using the galvanostatic charge-discharge strategy, the most reliable and accurate method for evaluating the supercapacitive properties of electrodes. Figure 10.5 shows the comparative current charge/discharge curves of the three BPPGE-SWCNT-MO electrodes

conducted in 1 M aqueous Na_2SO_4 and H_2SO_4 solutions at a current density of 0.1 Acm^{-2}, and potential range of - 0.2 to 0.8 V. The specific capacitance (SC) was obtained from Equations 10.2 and 10.3 [10]:

$$SC\ (Fcm^{-2}) = \frac{I \times \Delta t}{\Delta E \times A} \qquad (10.2)$$

$$SC\ (F\ g^{-1}) = \frac{I \times \Delta t}{\Delta E \times m} \qquad (10.3)$$

where I is the discharge current in ampere, Δt is the discharge time in second, ΔE is the discharge voltage in volt, A and m are the area and the mass of the electrode active material in cm^2 and g respectively. A is obtained from the peak corresponding to the respective metal oxide in ferri cyanide redox probe while the active mass m was obtained using the Sartorius CP225D micro-balance with an accuracy of 0.01 mg. The magnitude of SC obtained for the electrodes in 1 M Na_2SO_4 solution is in the order of BPPGE-SWCNT-NiO (140.0 $mFcm^{-2}$) > BPPGE-SWCNT-Co_3O_4 (79.8 $mFcm^{-2}$) > BPPGE-SWCNT-Fe_2O_3 (64.4 $mFcm^{-2}$). The SC values were higher (at the same current density) for the electrodes in H_2SO_4: BPPGE-SWCNT-NiO (186.0 $mFcm^{-2}$) > BPPGE-SWCNT-Co_3O_4 (117.8 $mFcm^{-2}$) > BPPGE-SWCNT-Fe_2O_3 (84.8 $mFcm^{-2}$). The magnitude of SC (Fg^{-1}) obtained for the electrodes in 1 M Na_2SO_4 solution is in the order of BPPGE-SWCNT-NiO (708 Fg^{-1}) > BPPGE-SWCNT-Co_3O_4 (399.0 Fg^{-1}) > BPPGE-SWCNT-Fe_2O_3 (322 Fg^{-1}). The SC values were higher (at the same current density) for the electrodes in H_2SO_4: BPPGE-SWCNT-NiO (928 Fg^{-1}) > BPPGE-SWCNT-Co_3O_4 (589 Fg^{-1}) > BPPGE-SWCNT-Fe_2O_3 (424 Fg^{-1}).

Table 10.1: Supercapacitive properties of the MO nanoparticles integrated with SWCNTs determined using cyclic voltammetry and galvanostatic discharge methods.

Electrode Modifier/Electrolyte	**Supercapacitive parameters**					
	Cyclic voltammetry (25 mVs^{-1})		**Galvanostatic discharge method (0.1 $mA\ cm^{-2}$)**			
	SC ($F\ g^{-1}$)	**SC ($mF\ cm^{-2}$)**	**SC ($F\ g^{-1}$)**	**SC ($mF\ cm^{-2}$)**	**SP ($W\ kg^{-1}$)**	**SE ($KW\ kg^{-1}$)**
SWCNT-NiO/ 1 M H_2SO_4	178.0±12.5	35.6±2.5	927.6±65.0	186.0±13.0	330.0±23.1	330.0±19.8
SWCNT-Co_3O_4 / 1 M H_2SO_4	82.5±5.8	16.5±1.2	588.5±41.2	117.8±8.3	440.0±30.8	440.0±27.1
SWCNT-Fe_2O_3 / 1 M H_2SO_4	79.0±5.5	15.8±1.1	424.0±29.7	84.8±5.9	490.0±34.3	490.0±29.3
SWCNT / 1 M H_2SO_4	33.0±2.3	6.6±0.5	-	-	-	-
SWCNT-NiO/ 1 M Na_2SO_4	198.0±13.9	39.6±2.8	707.7±49.5	140.0±9.8	374.0±26.2	374.0±26.2
SWCNT-Co_3O_4 / 1 M Na_2SO_4	36.0±2.5	7.2±0.5	399.0±28.0	79.8±5.6	450.0±32.2	450.0±21.4
SWCNT-Fe_2O_3 / 1 M Na_2SO_4	40.0±2.8	8.0±0.6	321.7±22.5	64.4±4.5	500.0±35.0	442.5±21.5
SWCNT / 1 M Na_2SO_4	36.0±2.0	7.2±0.3	-	-	-	-

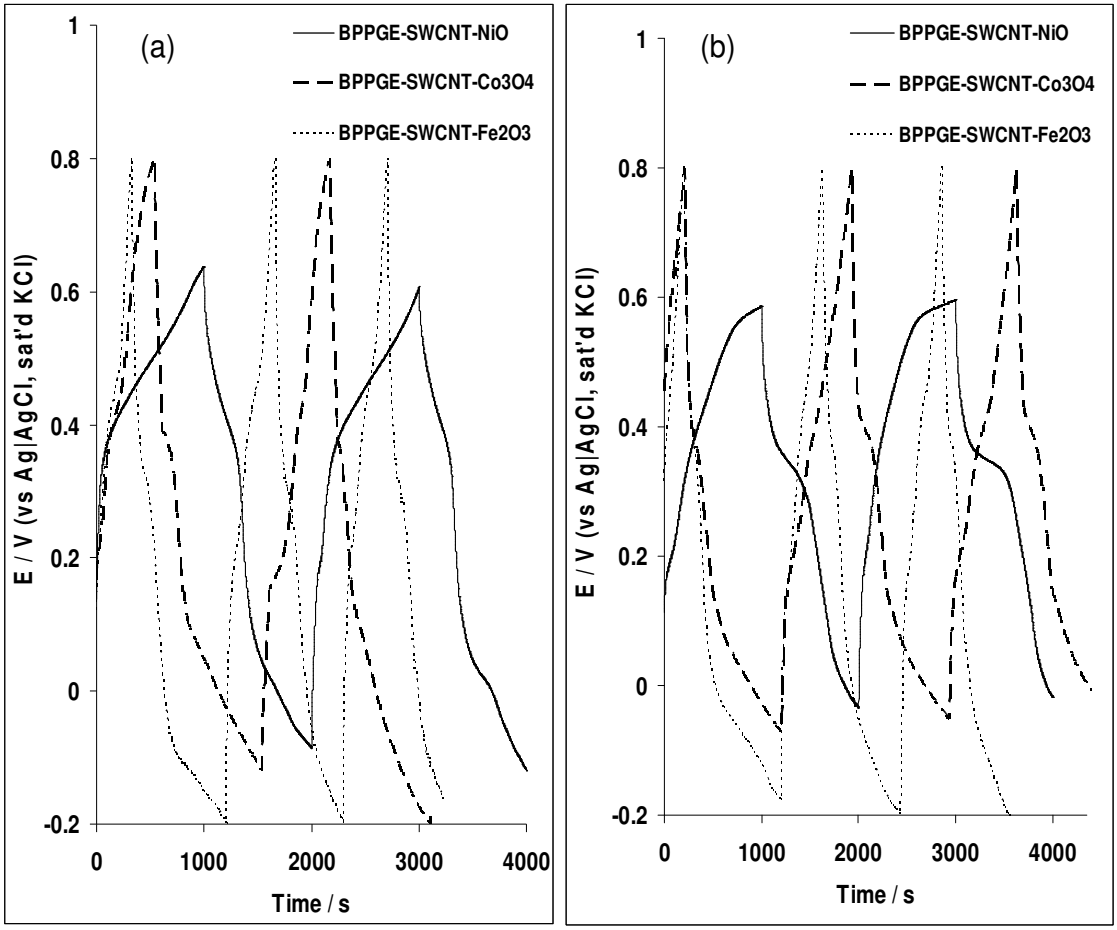

Figure 10.5: Typical examples of comparative galvanostatic charge discharge plot of the metal oxide SWCNTs/nanocomposite modified electrodes at an applied current density of 0.1 $mAcm^{-2}$ in (a) 1 M Na_2SO_4 and (b) 1 M H_2SO_4 aqueous electrolyte.

The values reported in this work are comparable or even higher than those reported in the literature using the same conditions (electrolytes and 3-electrode systems). For example, the values of 186 and 140 $mFcm^{-2}$ obtained for the BPPGE-SWCNT-NiO in 1 M H_2SO_4 and 1 M Na_2SO_4 respectively are greater than 96 and ~ 30 μFcm^{-2} reported for Fe_3O_4 nanofilm electrodeposited on gold

electrode in neutral environment [11], 27 $mFcm^{-2}$ reported for micro-polypyrrole (ppy) films doped with $ClO4^-$ (PPY_{ClO4}), prepared on Ni layers modified three-dimentional (3D) structures [12], 6.6 μFcm^{-2} obtained for carbon/zinc-aluminium (C-Zn_2Al) double layer hydroxide nanocomposite in 1 M H_2SO_4 [13], the 42 and 135.5 μFcm^{-2} reported for carbon/nickel-aluminium (C-Ni_2Al) layer double hydroxide (LDH) nanocomposite in 0.5 M Na_2SO_4 and 1 M $NaNO_3$ electrolyte respectively [14], or the value of 1117 μFcm^{-2} reported for the nitrogen-enriched carbon electrode described as 'extra-ordinary capacitor [15]. However, the result obtained in this study compares favourably with the recent report of 186 $mFcm^{-2}$ for nickel (II) octa [(3,5-bicarboxylate)-phenoxy] pthalocyanine integrated with functionalised single-walled carbon nanotubes (SWCNT-phenylamine) [16] and 112 $mFcm^{-2}$ for MWCNT-polyNiTAPc [17]. Also, these results are higher or comparable to literature values of 777 Fg^{-1} for MWCNT-polyNiTAPc in 1 M H_2SO_4 [17], 400 Fg^{-1} for polypyrrole [18,19], and a value of 616 Fg^{-1} for 3-methylthiophene using galvanostatic method [20]. The higher SC values obtained in this electrolyte may be attributed to its strong ionic nature, with greater diffusion, adsorption and storage capacity along the pores of the nanocomposites. One of the main reasons for the higher value obtained in this study may possibly be due to the stringent conditions adopted in functionalising the SWCNTs with carboxylic, phenolic and ketonic groups which make them more able to enhance ion mobility and storage, and also undergo both non-Faradaic (capacitive) and Faradaic (pseudocapacitive) reactions.

The specific power density (SP) and specific energy (SE) were easily estimated from the discharge process using Equations 10.4 and 10.5 [10,17,21]:

$$SP\ (Wkg^{-1}) = \frac{I \times \Delta E}{m} \qquad (10.4)$$

$$SE\ (WhKg^{-1}) = \frac{I \times t \times \Delta E}{m} \qquad (10.5)$$

where ΔE represents the potential range; other units retain their usual meaning. The SP and SE values are summarized in Table 10.1. The energy deliverable efficiency (η / %) of the best electrode film (BPPGE-SWCNT-NiO) was obtained from Equation 10.6 [21].

$$\eta\ (\%) = \frac{t_d}{t_c} \times 100 \qquad (10.6)$$

where t_d and t_c are discharge time and charging time, respectively. The energy deliverable efficiency for BPPGE-SWCNT-NiO is 99.9±9.0% and 99.9±9.4% in H_2SO_4 and Na_2SO_4, respectively. Since BPPGE-SWCNT-NiO electrode gave the highest capacitance, stability study of the electrode in Na_2SO_4 and H_2SO_4 was carried out at current density of 2 $mAcm^{-2}$ (Figure 10.6). Inset in Figure 10.6 represents some typical repetitive charge-discharge cycling for 1000 cycles, lasting about 3 days. The Figure clearly showed that the electrode is able to charge and discharge continuously without any significant loss in capacitance. Compared with the performance of the electrode in Na_2SO_4 (not shown), a better stability was observed in this electrolyte, showing about 5% loss of its initial specific capacitance after 100 cycle life in H_2SO_4, while an insignificant drop (about 0.1%) in SC value was noticed for the last 900 cycles. This indicates high stability characteristics of the SWCNT-NiO nanocomposites. Factors such as ionic strength, diffusion of ions and a favourable interaction between the ions and the nanoparticles

pores for complete ion insertion reaction may be some of the reasons for the observed phenomenon.

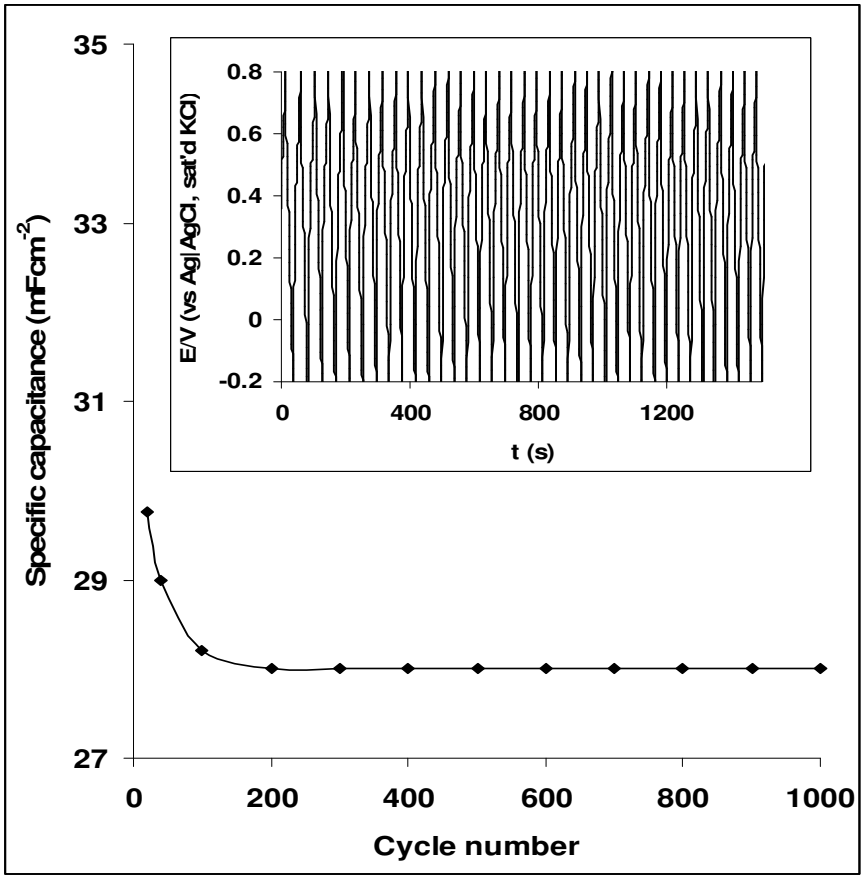

Figure 10.6: shows the effect of cycle number (1000) or cycle life on stability of BPPGE-SWCNT-NiO electrode in 1 M H_2SO_4 aqueous electrolytes. Inset is the typical examples of some of the charge-discharge curve (1000 cycles) for the BPPGE-SWCNT-NiO electrode in 1 M H_2SO_4 aqueous electrolytes.

10.4 Electrochemical impedance studies

Figure 10.7a and b presents the Nyquist plots obtained at a bias potential of 0.3 V for the three SWCNT-MO nanocomposites in 1 M Na_2SO_4 and H_2SO_4, respectively. The 0.3 V potential was chosen for

this experiment as the maximum capacitance was obtained at this potential.

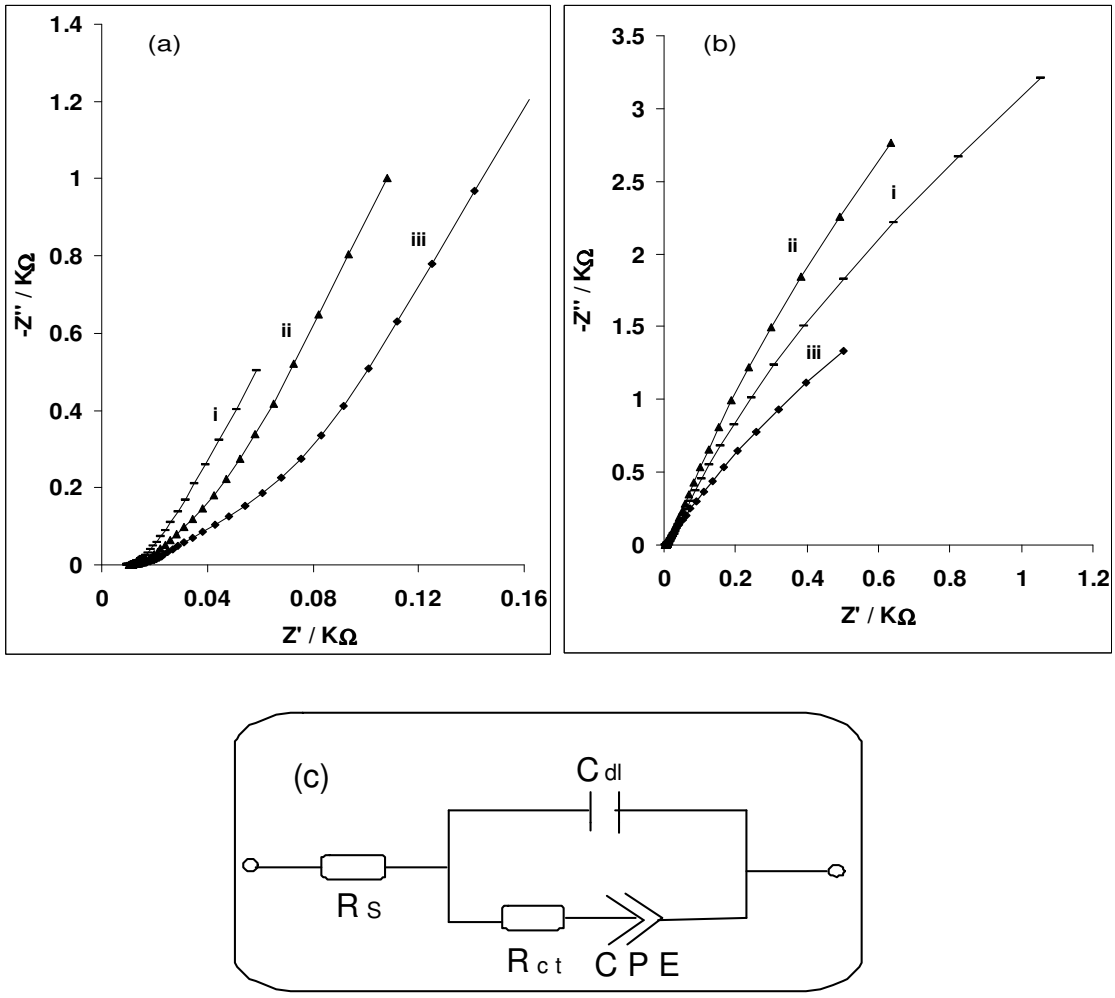

Figure 10.7: Typical Nyquist plots of (i) BPPGE-SWCNT-Fe_2O_3, (ii) BPPGE-SWCNT-NiO and (iii) BPPGE-SWCNT-Co_3O_4 electrodes in (a) 1 M Na_2SO_4 and (b) 1 M H_2SO_4 aqueous solutions at a fixed potential of 0.30 V vs Ag|AgCl sat'd KCl.

The low-frequency differential capacitance (C_d) for each of the electrodes can be obtained from the slope ($1/2\pi C_d$) of the plot of the

imaginary component of the impedance versus the reciprocal of the frequency (i.e., $-Z''$ vs $1/f$). The values of the SC for the three BPPGE-SWCNT-MO in 1 M Na_2SO_4 and H_2SO_4 were much smaller than values obtained using the galvanostatic discharge method. For example, the BPPGE-SWCNT-NiO gave approximately 7.7 and 4.7 $mFcm^{-2}$ in 1 M H_2SO_4 and Na_2SO_4, respectively. This discrepancy should perhaps not be surprising as other workers have observed similar behaviour, mainly for conducting polymers [22-31]. These workers have attributed the discrepancy to several factors such as the involvement of some physical and chemical heterogeneities [22], deeply trapped counter ions which remain immobile during impedance experiment [24], slow conformational changes occurring in the polymer network [26,27], or redox-switching hysteresis associated with conducting polymers [29]. Interestingly, SWCNTs have also been regarded as the ultimate polymeric material [31]. The impedance data were satisfactorily fitted, judged mainly by the values of the pseudo-χ^2 ($\leq 10^{-4}$) and relative % errors (Table 10.1), with the modified Randles electrical equivalent circuit model (Figure 10.7c).

Two important findings can be made from the impedance data. First, the R_{ct} values obtained for the electrodes in 1 M H_2SO_4 electrolyte are in the order: BPPGE-SWCNT-Co_3O_4 (0.18 Ωcm^2) < BPPGE-SWCNT-NiO (0.47 Ωcm^2) < BPPGE-SWCNT-Fe_2O_3 (0.99 Ωcm^2), indicating faster charge transport in the CoO and NiO based nanocomposites than the FeO-based electrode. Similar behaviour was observed in 1 M Na_2SO_4 (Table 10.1).

Table 10.2: Impedance data obtained for MO nanocomposite modified electrodes in 1 M H_2SO_4 and 1 M Na_2SO_4 electrolytes at a fixed potential of 0.30 V vs Ag|AgCl sat'd KCl.

Electrode	**Impedimetric parameters**					
	R_s (Ω cm	C_{dl} (μFcm^{-2})	R_{ct} (Ω cm^2)	CPE(μFcm^{-2})	*n*	*f^o (Hz)*
	1 M H_2SO_4					
BPPGE-SWCNT-NiO	0.46±0.01	69.70±4.3	0.47±0.0	1321.0±48.88	0.85±0.01	398.0
BPPGE-SWCNT-Co_3O_4	0.44±0.01	116.3±12.30	0.18±0.0	9334.0±14.00	0.80±0.01	199.5
BPPGE-SWCNT-Fe_2O_3	0.47±0.01	66.0±2.14	0.99±0.0	750.0±26.78	0.83±0.01	63.1
	1 M Na_2SO_4					
BPPGE-SWCNT-NiO	1.10±0.01	200.20±16.14	0.62±0.01	5963.0±231.36	0.89±0.01	199.5
BPPGE-SWCNT-Co_3O_4	1.13±0.01	107.50±8.99	0.83±0.01	3552.0±175.4	0.85±0.01	158.5
BPPGE-SWCNT-Fe_2O_3	0.98±0.01	702.0(6.57)	0.58±0.01	12070.0±511.1	0.90±0.01	125.9

The *n* values in the range 0.83 – 0.9 (Table 10.1) describe the porous nature of the electrodes, significant for the facile diffusion of ions to and from the electrode|solution interface.

Second, the transition point between the high frequency and low frequency component, referred to as the "knee" or "onset" frequency (f_o) describes the maximum frequency at which the capacity behaviour is dominant, and is a measure of the power capability of a supercapacitor; the higher the f_o the more rapidly the supercapacitor can be charged or the higher the power density that can be achieved from the supercapacitor [30,32]. As summarized in Table 10.1, the values of the f_o for the BPPGE-SWCNT-NiO are approximately 398 and 200 Hz in H_2SO_4 and Na_2SO_4, respectively. These values are greater than other electrodes, and again corroborate the high SC values of the electrode in H_2SO_4 solution. This means that the response time of the BPPGE-SWCNT-NiO (i.e., reciprocal of the f_o) is about 2.5 ms, suggesting that most of its stored energy is still accessible at frequencies as high as 398 Hz. Considering that even the most commercially available supercapacitors, including those specifically designed for higher power applications, operate at frequencies less than 1 Hz [33], the response time of this electrode is quite significant.

Since NiO nanocomposite modified electrode has the best SC from the three electrode system results above, the supercapacitive behaviour of chemically synthesised NiO integrated with MWCNT was investgated using two-electrode system in a coin cell type capacitor (already discussed in Chapter 2) for its potential commercial application. Figure 10.8 presents the cyclic voltammograms obtained for the symmetry (a) and (b); and the asymmetry (c) and (d) MWCNT-NiO based supercapacitor in 1 M H_2SO_4 and 1 M Na_2SO_4

aqueous electrolyte respectively at scan rate 5, 25, 50, 100, 200, 300, 400 and 500 mVs^{-1} (i-viii, inner to outer).

For the symmetric based electrode, there is a redox peaks at E_a ~ 0.80 V and E_c ~ 0.40 V due to the Ni(II)/Ni(III) redox process (Figure 10.8a). The ratio of the anodic and the cathodic current (I_{pa}/I_{pc}) is 1.0, which implies a favoured reversible or charge/discharge process of the supercapacitor material. On the other hand, in H_2SO_4, the asymmetry base supercapacitor showed an anodic peak at a lower potential (E_a ~ 0.57) and a weak cathodic peak at *ca* 0.50 V (Figure 10.8c). However as scan rate increases, the cathodic peak disappears while the anodic peak shift with increasing scan rate indicating a high capacitive behaviour. As scan rate increases, a large current separation with mirror images are observed at higher scan rate for both the symmetry and asymmetry supercapacitors. The CVs tend to be rectangular in H_2SO_4 than in Na_2SO_4. The specific capacitance (SC) was estimated from the cyclic voltammograms using Equation 10.1 above.

The capacitance values decreases with increasing scan rate (Table 10.3) with the highest values of 80 and 194 $mFcm^{-2}$ (obtained for the symmetry); and 950 and 220 $mFcm^{-2}$ obtained for the asymmetry supercapacitor in 1 M H_2SO_4 and 1 M Na_2SO_4 respectively (scan rate, 5 mVs^{-1}). The specific capacitance per mass of one cell electrode was calculated according to Equation 10.7 [34]:

$$\text{SC (F/g)} = 2\frac{C}{m} \qquad (10.7)$$

where C is the experimental measured capacitance of the supercapacitor, m is the mass of one composite electrode. The specific capacitance in F/g is represented in parenthesis in Table 10.3.

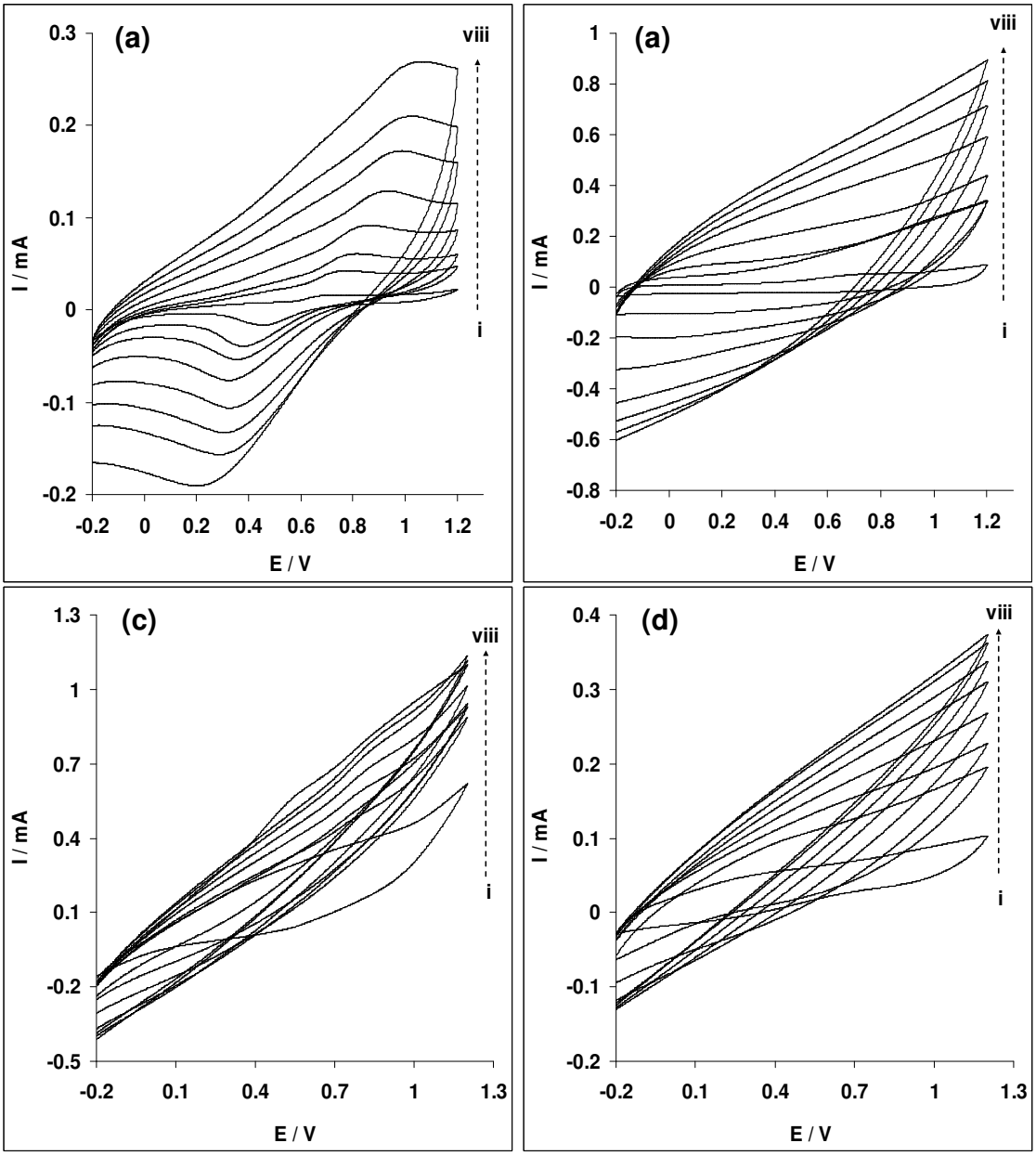

Figure 10.8: Cyclic voltammograms obtained for the symmetry (a) and (b); and the asymmetry (c) and (d) MWCNT-NiO baased supercapacitor (two–electrode cell) in 1 M H_2SO_4 and 1 M Na_2SO_4 aqueous electrolyte respectively at scan rate 5, 25, 50, 100, 200, 300, 400 and 500 mVs^{-1} (i-viii, inner to outer); mass of each electrode, 1.4 mg.

From Table 10.3, this result agreed with other reports where it was established that the asymmetry assembly gave higher specific capacitance values than the symmetry counterpart [34-38]. The results followed the same trend with those obtained by Ganesh et al. [35] but the highest value of 960 $mFcm^{-2}$ obtained at 5 mVs^{-1} is quite higher than the 83 $mFcm^{-2}$ obtained (at the same scan rate) for asymmetric supercapacitor cell assembly based on NiO in 6 M KOH [35]. The difference can be attributed to the different methods of obtaining the supercapacitor material and the well conducting and the mesoporous nature of MWCNT in enhancing charge flow in the nanocomposite used in this study. The equivalent specific capacitance value of 54.3 F/g at 5 mVs^{-1} is also greater compared with 34 and 27.67 F/g obtained at 2 and 5 mVs^{-1} respectively for an asymmetric NiO supercapacitor cell assembly in 6 M KOH electrolyte [35].

To further examine the detailed electrical properties or capacitive behaviour of the MWCNT-MO electrodes in the electrolytes, electrochemical impedance spectroscopy (EIS) experiment was conducted at $E_{1/2}$ of 0.55 V vs Ag|AgCl, sat'd KCl. Figure 10.9a presents the Nyquist plots obtained for the symmetry and the asymmetry assembly in both electrolytes. The Nyquist plots showed a good capacitor-like behaviour with a small diffusion limitation. Figures 10.9b – 10.9d are the equivalent electrical circuits' diagrams for fitting of the impedance data. The data obtained from the fittings are presented in Table 10.4, clearly showing satisfactory fitting as judged by the low relative errors.

Table 10.3: Specific capacitance ($mFcm^{-2}$) for the symmetric and asymmetric MWCNT-NiO based supercapacitor (two-electrode cell) in 1 M H_2SO_4 and 1 M Na_2SO_4 aqueous electrolyte respectively. Values in parenthesis are the specific capacitance in Fg^{-1}.

Scan rate (mVs^{-1})	**Specific capacitance ($mFcm^{-2}$)**		**Specific capacitance ($mFcm^{-2}$)**	
	MWCNT-NiO|H_2SO_4|NiO-MWCNT	**MWCNT-NiO|H_2SO_4|MWCNT**	**MWCNT-NiO|Na_2SO_4|NiO-MWCNT**	**MWCNT-NiO|Na_2SO_4|MWCNT**
5	80.0 (4.6 Fg^{-1})	950.0 (54.3 Fg^{-1})	194.0 (11.1 Fg^{-1})	220.0 (12.6 Fg^{-1})
25	40.0 (3.2)	450.0 (25.7)	152.0 (8.7)	92.0 (5.3)
50	27.5 (2.2)	160.0 (9.1)	110.0 (6.3)	47.5 (2.7)
100	21.2 (1.2)	65.0 (3.7)	62.5 (3.6)	30.0 (1.7)
200	15.0 (0.9)	41.6 (2.4)	47.5 (2.7)	16.3 (0.93)
300	12.5 (0.72)	29.6 (1.7)	34.2 (2.0)	11.7 (0.7)
400	11.9 (0.68)	24.6 (1.4)	30.6 (1.8)	10.0 (0.6)
500	12.0 (0.68)	21.4 (1.2)	28.0 (1.6)	7.0 (0.4)

Circuit 10.9b fitted impedance data obtained for the symmetry assembly in both 1 M H_2SO_4 and 1 M Na_2SO_4, while circuit 10.9c fitted the impedance data for the asymmetry assembly in 1 M H_2SO_4. Circuit 10.9d fitted the impedance data for the asymmetry assembly in 1 M Na_2SO_4. From Table 10.4, the assymetry supercapacitor, MWCNT-NiO|H_2SO_4|MWCNT has the lowest R_{ct} values (32.1 Ω or 1.28 Ωcm^{-2}) in 1 M H_2SO4. The result indicates faster charge transport of the supercapacitor, which also could be responsible for its high SC values. A phase angle of 31° and 21° are obtained for the symmtery (MWCNT-NiO|H_2SO_4|MWCNT-NiO) and asymmetry (MWCNT-NiO|H_2SO_4|MWCNT) supercapacitors respectively, indicating a pseudocapacitive behaviour. On the other hand, a phase angle of 11° and 52° are obtained for the symmtery (MWCNT-NiO|Na_2SO_4|MWCNT-NiO) and asymmetry (MWCNT-NiO|Na_2SO_4|MWCNT) supercapacitors respectively. A phase angle of 90° is expected for pure and ideal capacitive behaviour. The low-frequency differential capacitance (C_d) for the symmetric and the asymmetric electrodes in 1 M Na_2SO_4 and H_2SO_4 were much smaller than values obtained using the galvanostatic discharge method. The symmtery (MWCNT-NiO|H_2SO_4|MWCNT-NiO) gave approximately 3.58 and 2.58 $mFcm^{-2}$ in 1 M H_2SO_4 and Na_2SO_4 while the asymmetry (MWCNT-NiO|H_2SO_4|MWCNT) gave values of 3.08 and 2.17 $mFcm^{-2}$ in 1 M H_2SO_4 and Na_2SO_4 respectively. The discrepancy in the values has been discussed above.

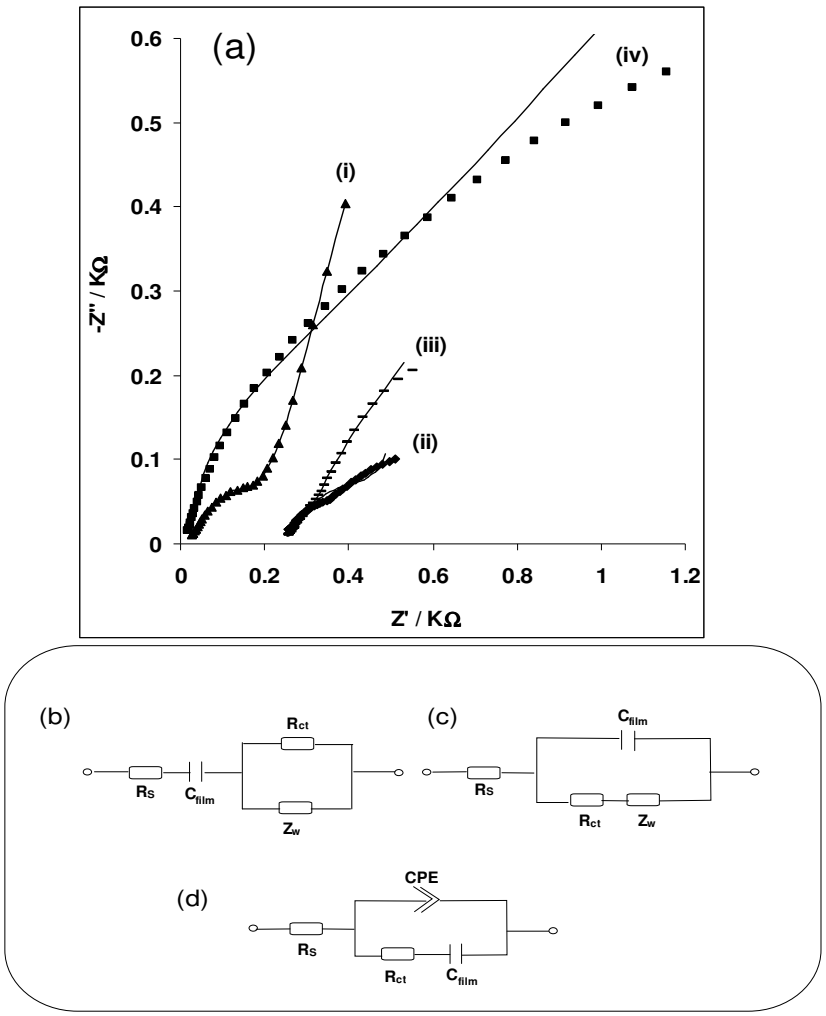

Figure 10.9: (a) Typical Nyquist plots obtained for symmetry: (i) MWCNT-NiO|H_2SO_4|MWCNT-NiO, (ii) MWCNT-NiO|Na_2SO_4|MWCNT-NiO;andthe asymmetry:(iii)MWCNT-NiO|H_2SO_4|MWCNT,(iv)MWCNT-NiO|Na_2SO_4|MWCNT supercapacitors at a fixed potential of 0.55 V vs Ag|AgCl sat'd KCl. Figures 5b-d are the circuit used for fitting the impedance data in (a). Circuit 10.9b fitted impedance data obtained for the symmetry assembly in both 1 M H_2SO_4 and 1 M Na_2SO_4, while circuit 10.9c fitted the impedance data for the asymmetry assembly in 1 M H_2SO_4. Circuit 10.9d fitted the impedance data for the asymmetry assembly in 1 M Na_2SO_4.

Table 10.4: Impedance data obtained for the symmetry and asymmetry MWCNT-NiO nanocomposite based supercapacitor (two-electrode cell) in 1.0 M H_2SO_4 and 1.0 M Na_2SO_4 electrolytes at a fixed potential of 0.55 V vs Ag|AgCl sat'd KCl.

Electrode	**Impedimetric parameters**					
	R_s (Ω cm^2)	**C_{dl} (μFcm^{-2})**	**R_{ct} (Ω cm^2)**	**CPE (μFcm^{-2})**	**n**	**Z_w (mΩ cm^2)**
MWCNT-NiO|H_2SO_4|MWCNT-NiO	2.15±0.03	1330.30±121.99	52.05±0.64	-	-	11.6±0.1
MWCNT-NiO|Na_2SO_4|MWCNT-NiO	24.73±0.02	1100.00±156.00	30.94±0.10	-	-	8.9±0.1
MWCNT-NiO|H_2SO_4|MWCNT	25.69±0.02	4.90±0.78	1.28±0.01	-	-	23.8±0.1
MWCNT-NiO|Na_2SO_4|MWCNT	-2.39±0.04	0.70±0.04	9.42±0.12	1308.0±84.1	0.33±0.01	-

The comparative current charge/discharge experiment of the supercapacitor cell assembly in (a) 1 M H_2SO_4 and (b) 1 M Na_2SO_4 electrolyte solutions at current density of 0.25 mA cm^{-2} was studied at potential range of - 0.2 to 0.8 V to observe the pseudocapacitance arising from the redox reaction at this voltage range. Figure 10.10 (symmetry) and Figure 10.11 (asymmetry) represent the charge/discharge curve obtained. It was observed that the charging-discharging time are almost the same. The specific capacitance of the supercapacitor (SC) was calculated using the Equation 10.3 above. The calculated SC is 277.8 $mAcm^{-2}$ (or 7.8 F/g) and 255.0 $mAcm^{-2}$ (or 7.2 F/g) for the symmetry supercapacitor in 1 M H_2SO_4 and 1 M Na_2SO_4 respectively. The values are higher, 925.9 $mAcm^{-2}$ (53.9 F/g) and 568.2 $mAcm^{-2}$ (15.9 F/g) for the asymmetry assembly in 1 M H_2SO_4 and 1 M Na_2SO_4 respectively. The SC values obtained from the charge-discharge experiment are slightly higher especially for the symmetry supercapacitor compared with those obtained from the CV experiment but there is a good correlation between the CV and galvanostatic measurements for the asymmetry cell. The SC value (53.9 F/g) recorded for the asymmetry MWCNT-NiO|H_2SO_4|MWCNT supercapacitor in H_2SO_4 is higher compared with 37 and 40 F/g reported for the symmetry (NiO|KOH|NiO) and the asymmetry (NiO|KOH|activated carbon) supercapacitors respectively using same technique [35]. Aside the fact that the high capacitance of the MWCNT-NiO has been related to the possible consequence of its high surface area and quality pore networks, the higher SC values in H_2SO_4 observed in this study can also be attributed to the strong ionic nature of the H_2SO_4 electrolyte among other factors already mentioned above.

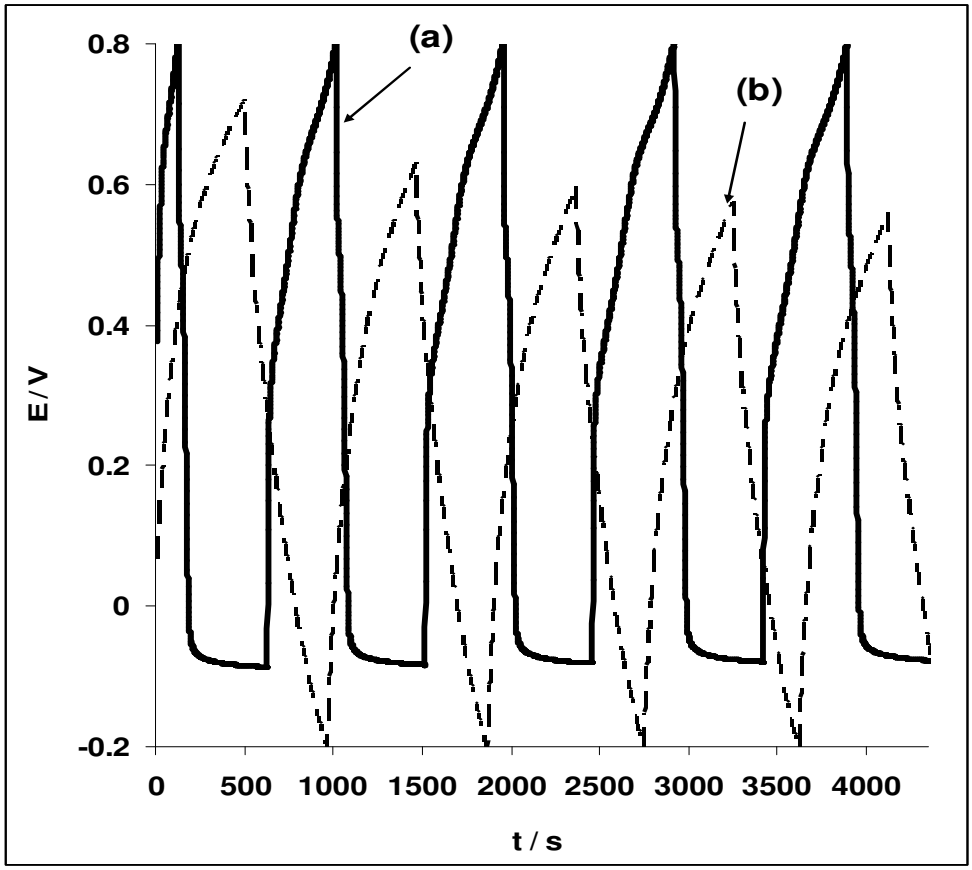

Figure 10.10: Typical examples of galvanostatic charge discharge profile of the symmetry MWCNT-NiO based supercapacitor (two-electrode cell) in (a) 1 M H_2SO_4 and (b) 1 M Na_2SO_4 aqueous electrolytes, at an applied current density of 0.25 $mAcm^{-2}$.

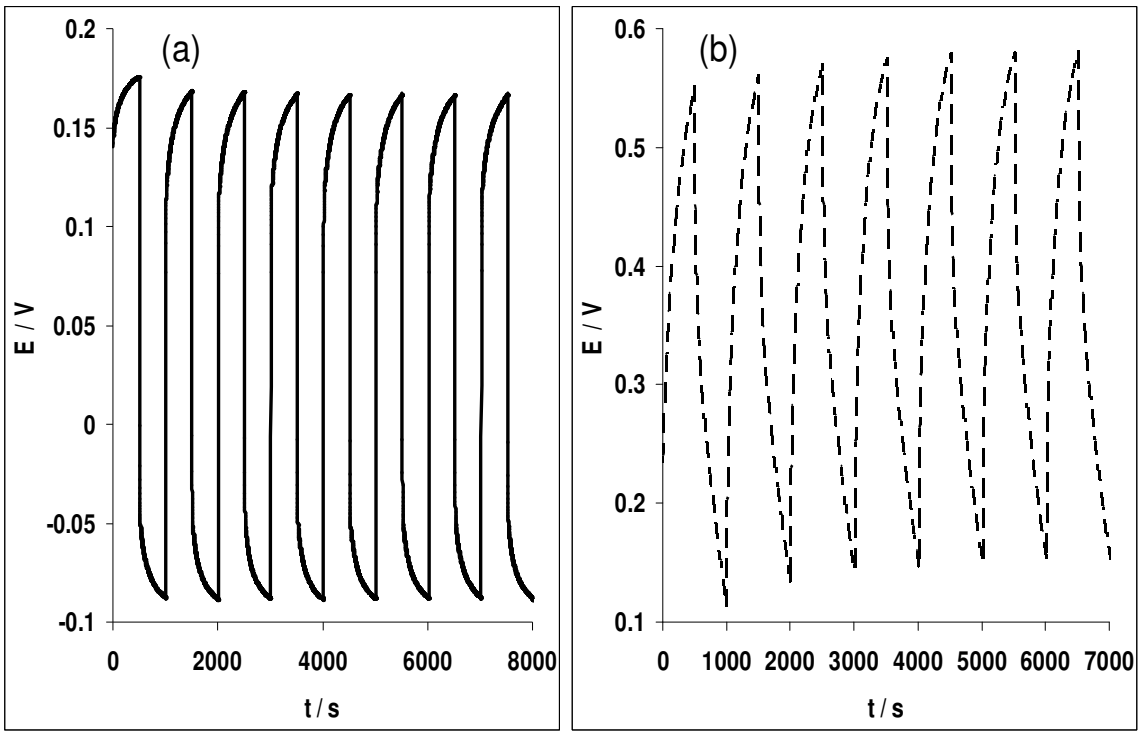

Figure 10.11: Typical examples of galvanostatic charge discharge profile of the asymmetry MWCNT-NiO bases supercapacitor (two-electrode cell) in (a) 1 M H_2SO_4 and (b) 1 M Na_2SO_4 aqueous electrolytes, at an applied current density of 0.25 $mAcm^{-2}$.

Since the asymmetry MWCNT-NiO|H_2SO_4|MWCNT cell gave the highest capacitance, its SP, SE and the energy deliverable efficiency (η / %) are estimated as 3.8 Wkg^{-1} and 1.9 $KWhKg^{-1}$ and 101.0±8.1% respectively using Equations 10.4, 10.5 and 10.6. The stability of the cell at a current density of 2.5 $mAcm^{-2}$ was also investigated. A typical repetitive charge-discharge cycling for 1000 cycles, lasting about 24 h is shown in Figure 10.12. The electrode is able to charge and discharge continuously without any significant loss (< 5 %) SC value was noticed for the last 900 cycles. The electrode stability was attributed to the contribution of the chemical stability of MWCNT in the nanocomposite.

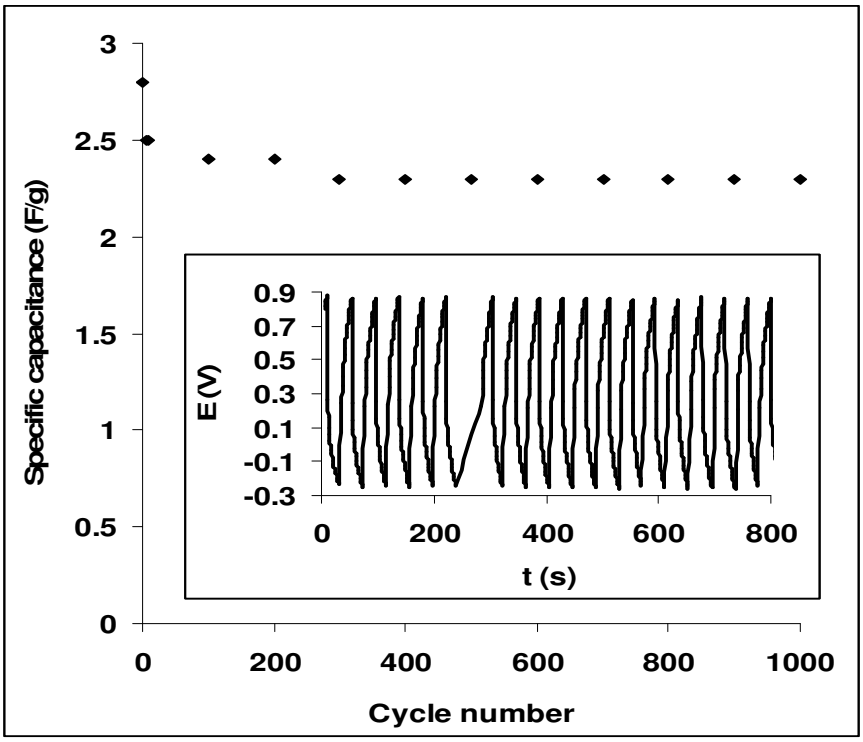

Figure 10.12: Cyclic life (1000 cycles) of the asymmetry MWCNT-NiO |H_2SO_4|MWCNT supercapacitor showing the stability in 1 M H_2SO_4 aqueous electrolytes. Inset is the section of the charge-discharge curves obtained for the electrodes at applied current density of 2.5 mAcm^2.

This study showed that SWCNT-NiO nanocomposite modified electrode exhibits remarkable supercapacitive behaviour in neutral and acidic media compared to SWCNT-Fe_2O_3 and SWCNT-Co_3O_4 counterparts. Interestingly, the capacitive behaviour of the SWCNT-NiO was more enhanced in a H_2SO_4 solution than the Na_2SO_4 electrolyte. Asymmetry assembly of MWCNT-NiO|H_2SO_4|MWCNT gave the highest specific capacitance value compared with the symmetric conterpart. Both the SWCNT-NiO electrode and the MWCNT-NiO|H_2SO_4|MWCNT supercapacitor maintained good stability with less than 5% loss of their specific capacitance after 1000 cycles.

References

1. N.S. NcIntyre, M.G. Cook, *Anal. Chem.* 47 (1975) 2208.

2. S. Sunohara, K. Nishimura, K. Yahikozawa, M. Ueno, *J. Electroanal. Chem.* 161 (1993) 354.

3. J-K. Chang, M-T. Lee, C-H. Huang, W-T. Tsai, *Mater. Chem. Phys.* 108 (2008) 124.

4. R.C. Chikate, K-W. Jun, C.V. Rode, *Polyhedron* 27 (2008) 933.

5. A. Salimi, H. Mamkhezri, R. Hallaj, S. Soltanian, *Sens. Actuators B* 129 (2008) 246.

6. H-S. Choo, T. Kinumoto, M. Nose, K. Miyazaki, T. Abe, Z. Ogumi, *J. Power sources* 185 (2008) 740.

7. A.L.M. Reddy, S. Ramaprabhu, *J. Phys. Chem. C* 111 (2007) 7727.

8. M. S. Wu, H-H Hsieh, *Electrochim. Acta* 53 (2008) 3427.

9. J. Pillay, K. I. Ozoemena, *Chem. Phys. Lett.* 441 (2007) 72.

10. T. Shinomiya, V. Gupta, N. Miura, *Electrochim. Acta* 51 (2006) 4412.

11. S.Y. Wang, K.C. HO, S.L. Kuo, N.L. Wu, *J. Electrochem. Soc.* 153 (2006) A75.

12. W. Sun, X. Chen, *J. Power Sources* 193 (2009) 924.

13. F. Leroux, E. Raymundo-Pinero, J-M. Nedelec, F. Beguin, *J. mater. Chem.* 16 (2006) 2074.

14. T. Stimpfling, F. Leroux, *Chem. Mater.* 22 (2010) 974.

15. D. Hulicova-Jurcakova, M. Kodama, S. Shiraishi, H. Hatori, Z.H. Zhu, G.Q. Lu, *Adv. Funct. Mater.* 19 (2009) 1.

16. B.O. Agboola, K.I. Ozoemena, *J. Power Sources* 195 (2010) 3841.

17. A.T. Chidembo, K.I. Ozoemena, B.O. Agboola, V. Gupta, G.G. Wildgoose, R.G. Compton, *Energy Environ. Sci.* 3 (2010) 228.
18. E. Frackowiak, K. Jurewicz, S. Delpeux, F. Beguin., *J. Power Sources* 97 (2001) 822.
19. R.K. Sharma, A.C. Rastogi, S.B. Desu, *Electrochem. Commun.* 10 (2008) 268.
20. C.P. Fonseca, J.E. Benedetti, S. Neves, *J. Power Sources* 158 (2006) 789.
21. S. G. Kandalkar, J. I. Gunjakar, C. D. Lokhande, *Appl. Surf. Sci.,* 254 (2008) 5540.
22. B.J. Feldman, P. Burgmayer, R.W. Murray, *J. Am. Chem. Soc.* 107 (1985) 872.
23. N. Mermilliod, J. Tanguy, F. Petior, *J. Electrochem. Soc.* 133 (1986) 1073.
24. J. Tanguy, N. Mermilliuod, M. Hoclet, *J. Electrochem. Soc.* 134 (1987) 795.
25. T. Tanguy, M. Slama, M. Hoclet, J.L. Baudin, *Synth. Met.* 28 (1989) 145.
26. M. Kalaji, L.M. Peter, *J. Chem. Soc. Faraday Trans.* 87 (1991) 853.
27. X. Ren, P.G. Pickup, *J. Electroanal. Chem.* 372 (1994) 289.
28. T.C. Girija, M.V. Sangaranarayanan, *J. Appl. Electrochem.* 36 (2006) 531.
29. G. Xu, W. Wang, X. Qu, Y. Yin, L. Chu, B. He, H. Wu, J. Fang, Y. Bao, L. Liang, *Eur. Polym. J.* doi :10.1016/j.europolymj.2009.05.016.
30. C. Du, N. Pan, *J. Power Sources* 160 (2006) 1487.
31. M.J. Green, N. Behabtu, M. Pasquali, W.W. Adams, *Polymer* 2009.(doi:10.1016/j.polymer.2009.07.044).

32. C-W. Huang, Y-T. Wu, C-C. Hu, Y-Y. Li, *J. Power Sources* 172 (2007) 460.

33. Miller JR, Proceedings of the Electrochemical Society Meeting, Chicago, October, 1995, 246.

34. V. Khomenko, E. Frackowiak, F. Beguin, *Electrochim. Acta* 50 (2005) 2499.

35. V. Ganesh, S. Pitchumani, V. Lakshminarayanan, *J. Power Sources* 158 (2006) 1523.

36. H.-Q. Wang, Z.-S. Li, Y.-G. Huang, Q.-Y. Li, X.-Y. Wang, *J. mater. Chem.*, 2010|DOI:10.1039/c000339e.

37. Q. Wang, Z. Wen, J. Li, *Adv. Funct. Mater.* 16 (2006) 2141.

38. Q.T. Qu, Y. Shi, S. Tian, Y.H. Chen, Y.P. Wu, R. Holze, J. *Power Sources* 194 (2009) 1222.